

## Supporting Information

### Self-Inhibitory Electron Transfer of the Co(III)/Co(II)-Complex Redox Couple at Pristine Carbon Electrode

Ran Chen,<sup>†</sup> Amin Morteza Najarian,<sup>‡</sup> Niraja Kurapati,<sup>†</sup> Ryan J. Balla,<sup>†</sup> Alexander Oleinick,<sup>¶</sup> Irina Svir,<sup>¶</sup>  
Christian Amatore,<sup>¶,#</sup> Richard L. McCreery,<sup>‡</sup> and Shigeru Amemiya<sup>†,\*</sup>

<sup>†</sup> *Department of Chemistry, University of Pittsburgh, 219 Parkman Avenue, Pittsburgh, Pennsylvania,  
15260, United States*

<sup>‡</sup> *Department of Chemistry, University of Alberta, Edmonton, Alberta T6G 2R3, Canada*

<sup>¶</sup> *PASTEUR, Département de chimie, École normale supérieure, PSL University, Sorbonne Université,  
CNRS, 75005 Paris, France*

<sup>#</sup> *State Key Laboratory of Physical Chemistry of Solid Surfaces, College of Chemistry and Chemical  
Engineering, Xiamen University, Xiamen, 361005, China*

\* To whom correspondence should be addressed: amemiya@pitt.edu.

|                 |  |
|-----------------|--|
| <b>Contents</b> | 1. Simulation and additional results of SECM-based nanogap voltammetry                               |
|                 | 2. Simulation and additional results of cyclic voltammetry   |
|                 | 3. Models for effective sizes of Co(phen) <sub>3</sub> <sup>2+</sup> and Frumkin double-layer effect |

**SECM Model.** Here we define a theoretical model to quantitatively describe SECM-based nanogap voltammograms of the  $\text{Co(phen)}_3^{3+/2+}$  couple in feedback and SG/TC modes. We consider an SECM configuration in the cylindrical coordinates (Figure S1) to define the following diffusion problem.

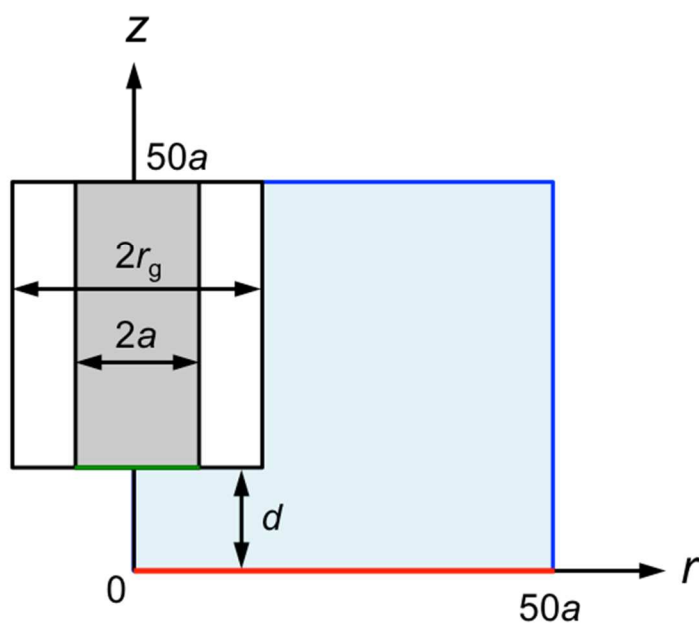


**Figure S1.** Scheme of the SECM configuration with a glass-insulated Pt tip ( $RG = 2$ ) positioned over a macroscopic eC substrate. The red boundary represents the eC surface. The green boundary represents the tip surface. Black boundaries are insulating or a symmetry axis. Blue boundaries represent the bulk solution.

A model for SECM-based nanogap voltammetry is based on the adsorption of A ( $= \text{Co(phen)}_3^{2+}$ ), that proceeds its oxidation to B ( $= \text{Co(phen)}_3^{3+}$ ), as given by



The respective equations are equivalent to eqs 1 and 2. Diffusion equations for species,  $i$  ( $= A$  or  $B$ ), is given in the cylindrical coordinates (Figure S1) to yield

$$\frac{\partial c_i}{\partial t} = D_i \left[ \frac{\partial^2 c_i}{\partial r^2} + \frac{1}{r} \frac{\partial c_i}{\partial r} + \frac{\partial^2 c_i}{\partial z^2} \right] \quad (\text{S-3})$$

where  $D_i$  is the diffusion coefficient of species  $i$  ( $= A$  or  $B$ ). The rate of the electron-transfer (ET) reaction,  $v_{\text{et}}$ , is given by

$$v_{\text{et}} = k_{\text{red}} c_B - k_{\text{ox}} c_A \quad (\text{S-4})$$

where  $c_A$  and  $c_B$  represents the concentrations of non-adsorbed species  $A$  and  $B$  near the electrode surface, respectively. The adsorption rate of  $A$ ,  $v_{\text{ads}}$ , is given by

$$v_{\text{ads}} = k_{\text{ads}} c_A (\Gamma_s - \Gamma_A) - k_{\text{des}} \Gamma_A \quad (\text{S-5})$$

with

$$k_{\text{ads}} = k_{\text{ads}}^0 \exp(2\alpha_{\text{ads}} g \Gamma_A / RT) \quad (\text{S-6})$$

$$k_{\text{des}} = k_{\text{des}}^0 \exp[-2(1 - \alpha_{\text{ads}}) g \Gamma_A / RT] \quad (\text{S-7})$$

where  $\Gamma_A$  is the surface concentration of adsorbed species  $A$ ,  $k_{\text{ads}}^0$  and  $k_{\text{des}}^0$  are standard adsorption and desorption rate constant,  $g$  is the energy of interaction between adsorbed molecules, and  $\alpha_{\text{ads}}$  is a symmetry coefficient ( $0 < \alpha_{\text{ads}} < 1$ ) regulating the effect of  $g$  on the adsorption activation barrier. Adsorption equilibrium is achieved at  $t = 0$  to yield eq 8 with  $\beta = k_{\text{ads}}^0 / k_{\text{des}}^0$ . Accordingly, boundary conditions at the substrate surface are given by

$$-D_A \left[ \frac{\partial c_A}{\partial z} \right]_{z=0} = v_{\text{et}} - v_{\text{ads}} \quad (\text{S-8})$$

$$-D_B \left[ \frac{\partial c_B}{\partial z} \right]_{z=0} = -v_{\text{et}} \quad (\text{S-9})$$

$$\left[ \frac{\partial \Gamma_A}{\partial t} \right] = v_{\text{ads}} \quad (\text{S-10})$$

Boundary conditions at the tip depend on the operation mode, i.e.,  $c_A = 0$  in the feedback mode and  $c_B = 0$  in the SG/TC mode. In either operation mode, a current response at the tip,  $i_T$ , is given by

$$i_T = 2\pi F \int_0^a r v_{\text{et}} dr \quad (\text{S-11})$$

**Dimensionless SECM Model.** Diffusion equations for species  $i$  ( $= A$  or  $B$ ) are defined by using the following dimensionless parameters and solved by using a commercial finite element simulation package, Multiphysics 5.3a (COMSOL, Burlington, MA). Specifically, diffusion equations in dimensionless forms are defined from eq S-3 for species  $i$  ( $= A$  or  $B$ ) as

$$\frac{\partial C_i}{\partial \tau} = \gamma_i \left[ \frac{\partial^2 C_i}{\partial R^2} + \frac{1}{R} \frac{\partial C_i}{\partial R} + \frac{\partial^2 C_i}{\partial Z^2} \right] \quad (\text{S-12})$$

with

$$C_i = c_i / c_0 \quad (\text{S-13})$$

$$R = r / a \quad (\text{S-14})$$

$$Z = z / a \quad (\text{S-15})$$

$$\tau = D_A t / a^2 \quad (\text{S-16})$$

$$\gamma_i = D_i / D_A \quad (\text{S-17})$$

In addition, the potential sweep rate,  $v$ , is converted to the dimensionless form,  $\sigma$ , as

$$\sigma = a^2 v F / D_A R T \quad (\text{S-18})$$

Importantly, mass transport across the tip–substrate gap maintains a quasi-steady state when  $\sigma < 1$ .

Boundary conditions at the substrate surface (eqs S-8–S-10) are given by using dimensionless rates,

$V_{\text{et}}^{\text{SECM}}$  and  $V_{\text{ads}}^{\text{SECM}}$ , as

$$\left[ \frac{\partial C_A}{\partial Z} \right]_{Z=0} = V_{\text{et}}^{\text{SECM}} - V_{\text{ads}}^{\text{SECM}} \quad (\text{S-19})$$

$$\left[ \frac{\partial C_B}{\partial Z} \right]_{Z=0} = -\frac{V_{\text{et}}^{\text{SECM}}}{\gamma_i} \quad (\text{S-20})$$

$$\left[ \frac{\partial \theta_A}{\partial \tau} \right] = \frac{V_{\text{ads}}^{\text{SECM}}}{K_{\text{SECM}}} \quad (\text{S-21})$$

with

$$\theta_A = \Gamma_A / \Gamma_s \quad (\text{S-22})$$

$$K_{\text{SECM}} = \Gamma_s / ac_0 \quad (\text{S-23})$$

$$L = d / a \quad (\text{S-24})$$

Each dimensionless rate is given as follows. The dimensionless ET rate,  $V_{\text{et}}^{\text{SECM}}$ , is given by

$$V_{\text{et}}^{\text{SECM}} = \Lambda_{\text{het}}^{\text{SECM}} \left[ (\theta_{\text{ET}})^{-\alpha_{\text{ET}}} C_B - (\theta_{\text{ET}})^{1-\alpha_{\text{ET}}} C_A \right] \quad (\text{S-25})$$

with

$$\Lambda_{\text{het}}^{\text{SECM}} = k^0 a / D_A \quad (\text{S-26})$$

$$\theta_{\text{ET}} = \exp \left[ \frac{F(E - E_{\text{initial}})}{RT} \right] / \exp \left[ \frac{F(E^0 - E_{\text{initial}})}{RT} \right] \quad (\text{S-27})$$

where  $F(E^0 - E_{\text{initial}}) / RT$  serves as a scaling factor. The adsorption rate is defined in the dimensionless

form,  $V_{\text{ads}}^{\text{SECM}}$ , as

$$V_{\text{ads}}^{\text{SECM}} = \Lambda_{\text{ads}}^{\text{SECM}} (\theta_{\text{ads}})^{\alpha_{\text{ads}}} C_{\text{A}} (1 - \theta_{\text{A}}) - \Lambda_{\text{des}}^{\text{SECM}} (\theta_{\text{ads}})^{\alpha_{\text{ads}} - 1} \theta_{\text{A}} \quad (\text{S-28})$$

with

$$\Lambda_{\text{ads}}^{\text{SECM}} = k_{\text{ads}}^0 \Gamma_s a / D_{\text{A}} \quad (\text{S-29})$$

$$\Lambda_{\text{des}}^{\text{SECM}} = k_{\text{des}}^0 \Gamma_s a / c_0 D_{\text{A}} \quad (\text{S-30})$$

$$\theta_{\text{ads}} = \exp(g' \theta_{\text{A}}) \quad (\text{S-31})$$

$$g' = 2g\Gamma_s / RT \quad (\text{S-32})$$

The corresponding initial condition is given by

$$\frac{\Lambda_{\text{ads}}^{\text{SECM}}}{\Lambda_{\text{des}}^{\text{SECM}}} = \frac{\theta_{\text{A}}}{1 - \theta_{\text{A}}} \exp(-g' \theta_{\text{A}}) \quad (\text{S-33})$$

Finally, a normalized tip current response,  $I_{\text{T}}$ , is given by

$$I_{\text{T}} = \frac{i_{\text{T}}}{FD_{\text{A}} c_0 a} = \int_0^1 (2\pi R V_{\text{et}}) dR \quad (\text{S-34})$$

where the integral is calculated by COMSOL.

**Effects of Adsorption Kinetics on Nanogap Voltammograms.** We varied  $\Lambda_{\text{ads}}^{\text{SECM}}$  (eq S-29) to find that an experimental nanogap voltammogram deviates from simulated one with  $\Lambda_{\text{ads}}^{\text{SECM}} \leq 0.1$  (Figure S2). The low  $\Lambda_{\text{ads}}^{\text{SECM}}$  values deviate the adsorption process from the Frumkin isotherm (Figure S3).

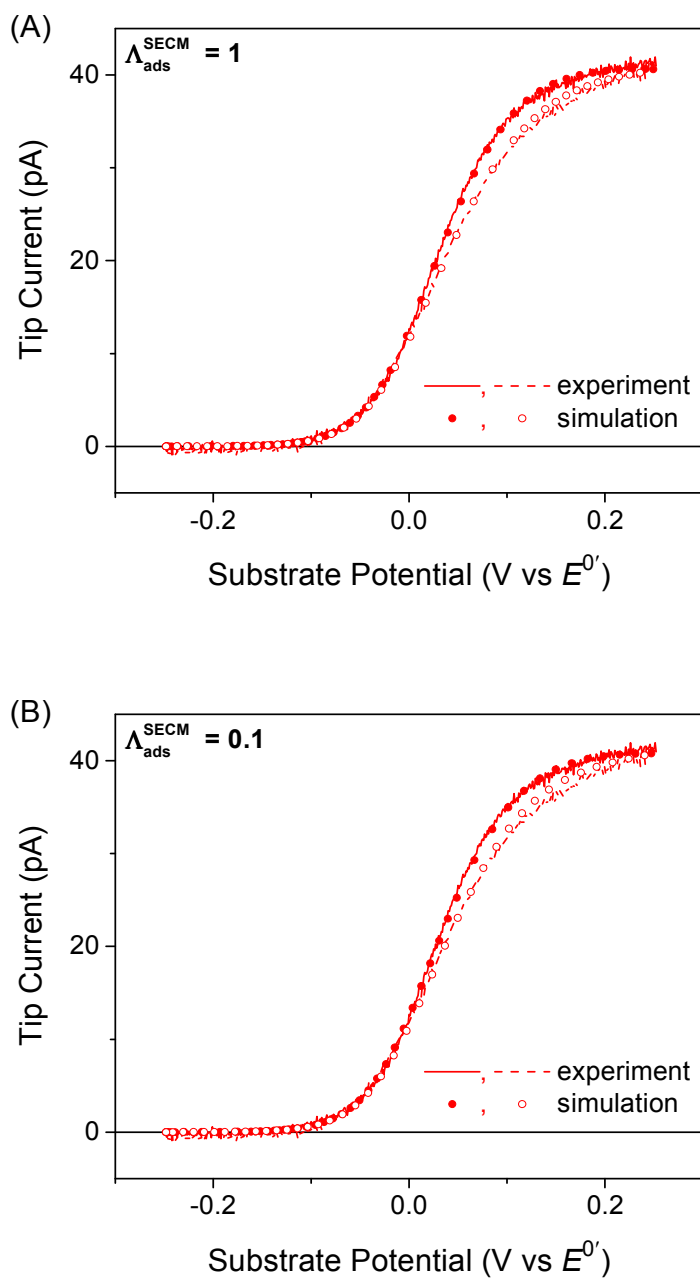


**Figure S2.** Experimental (lines) and simulated (circles) nanogap voltammograms of 0.1 mM  $\text{Co(phen)}_3^{2+}$  at an eC electrode in 1 M KCl as obtained by using a 1.0  $\mu\text{m}$ -diameter Pt tip in the SG/TC mode. Simulation employed  $\Lambda_{\text{ads}}^{\text{SECM}} =$  (A) 1 and (B) 0.1. Solid lines and closed circles represent the forward scan. Dashed lines and open circles correspond to the reverse scan.

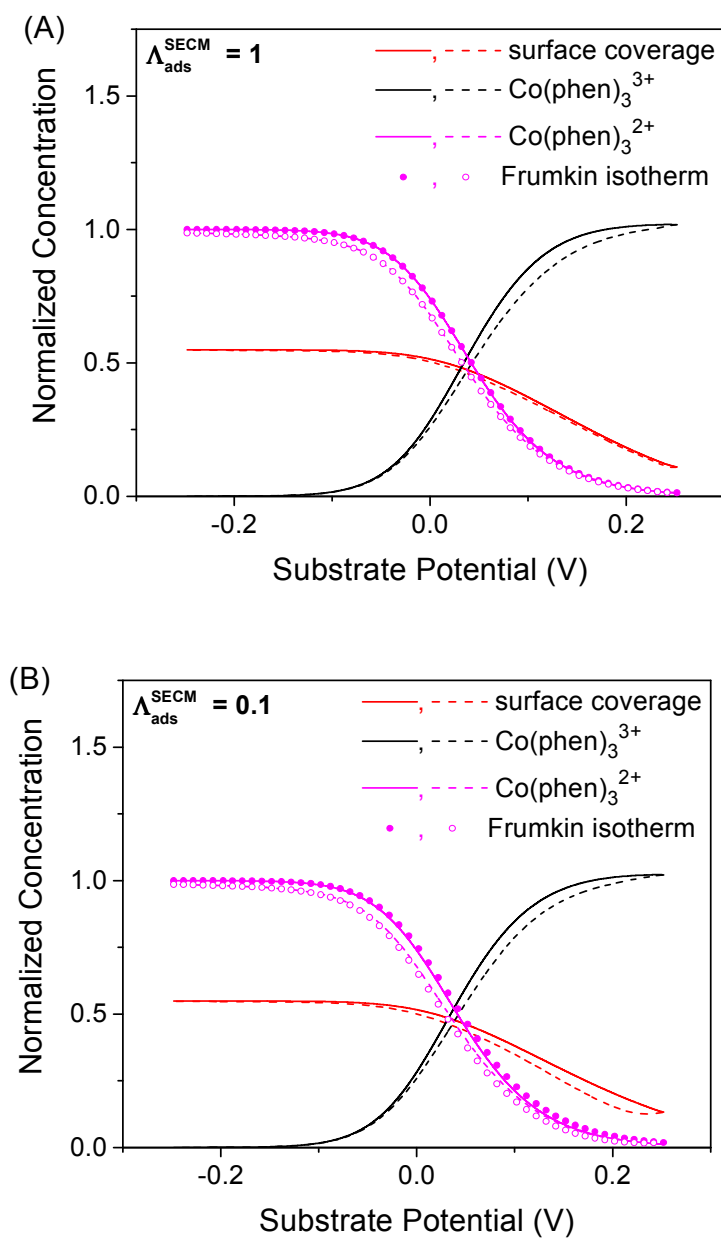


**Figure S3.** Normalized concentrations of redox species at the electrode/solution interface as simulated for SECM-based nanogap voltammetry in the SG/TC mode. Simulation employed  $\Lambda_{\text{ads}}^{\text{SECM}} =$  (A) 1 and (B) 0.1. in addition to parameters that are identical to those employed in Figure S2. Solid lines and closed circles represent the forward scan. Dashed lines and open circles correspond to the reverse scan.

**Effect of Electron-Transfer Kinetics on  $\text{Co(phen)}_3^{2+}$  Desorption.** We employed the finite element method to demonstrate that surface coverage decreases only to 0.56 at the switching potential when the oxidation of 1.0 mM  $\text{Co(phen)}_3^{2+}$  slows down owing to a stronger self-inhibitory effect (Figure S4). By contrast, surface coverage nearly dropped to zero when 0.1 mM  $\text{Co(phen)}_3^{2+}$  was oxidized faster owing to a weaker self-inhibitory effect (Figure 4).

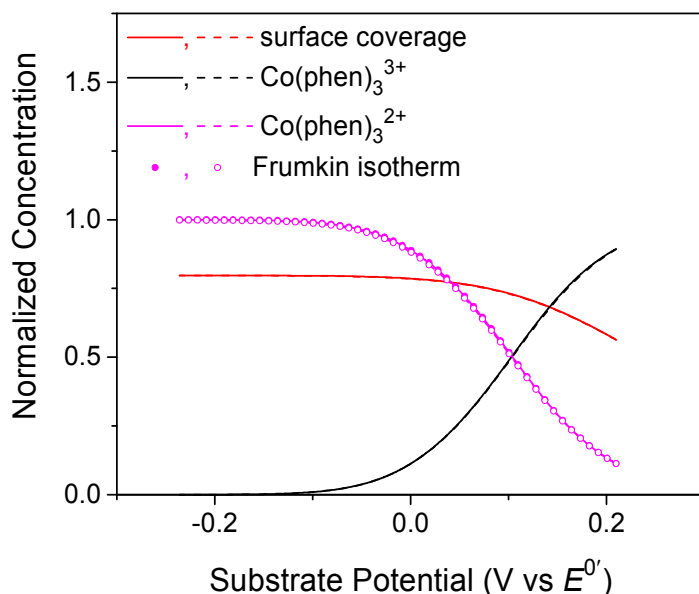


**Figure S4.** Normalized concentrations of redox species at the electrode/solution interface as simulated for the SG/TC mode. Parameters are identical to those employed in Figure 6C with  $d = 229$  nm. Solid lines and closed circles represent the forward scan. Dashed lines and open circles correspond to the reverse scan.

**Effect of KCl Concentrations on Nanogap Voltammograms.** Nanogap voltammograms of 0.1 and 0.3 mM  $\text{Co(phen)}_3^{2+}$  in 0.1 M KCl (Figure S5A and S5B, respectively) were measured and analyzed using adsorption parameters in Table 1 and adjusting  $k_0$  values.

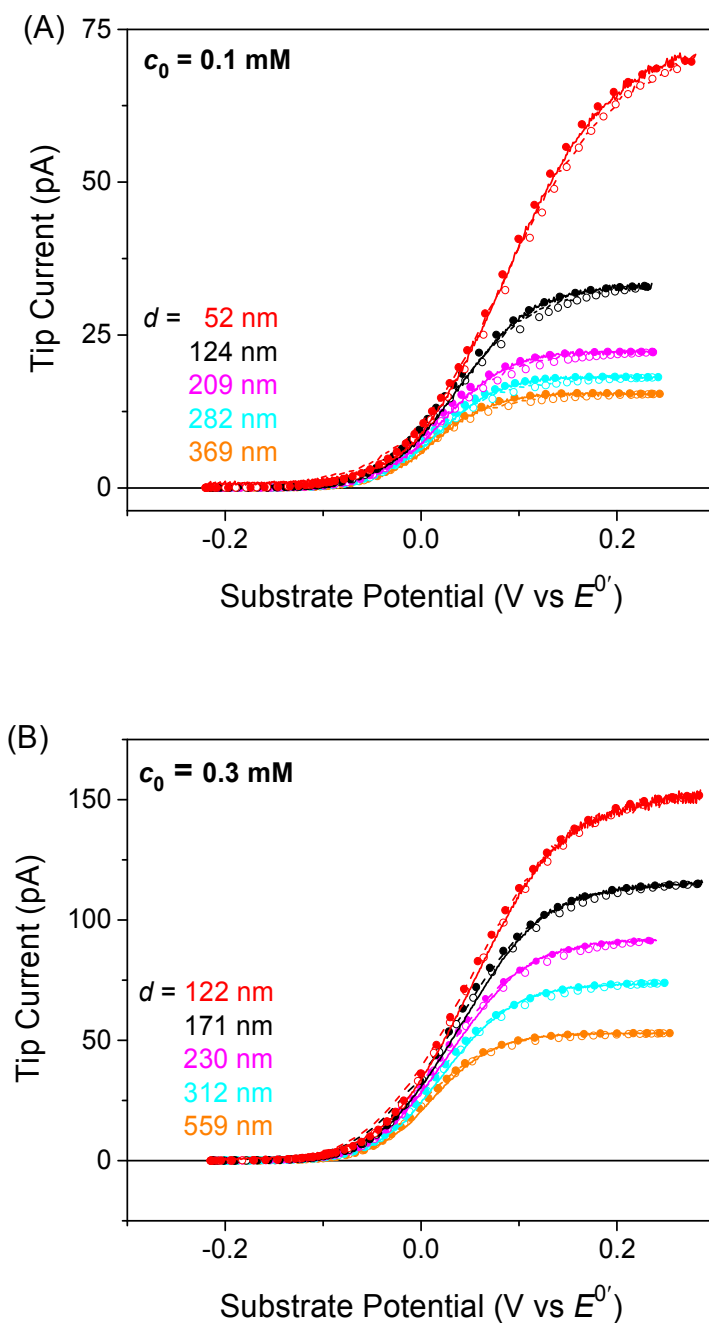


**Figure S5.** Experimental (lines) and simulated (circles) nanogap voltammograms of  $\text{Co(phen)}_3^{2+}$  at eC electrodes in 0.1 M KCl as obtained by using Pt tips with diameters of (A) 1.1 and (B) 1.3  $\mu\text{m}$  in the SG/TC mode. Solid and dashed lines represent forward and reverse scans, respectively. Open and closed circles are simulated voltammograms that yield best fits for forward and reverse scans, respectively.

**CV Model.** Here we consider a model for CV by considering the adsorption of A (eq S-1) and its preceding oxidation to B (S-2). Diffusion equation for species,  $i$  (= A or B), is given by

$$\frac{\partial c_i}{\partial t} = D_i \left[ \frac{\partial^2 c_i}{\partial z^2} \right] \quad (\text{S-35})$$

Boundary conditions at the eC surface are given by

$$D_A \left[ \frac{\partial c_A}{\partial z} \right]_{z=0} = v_{\text{et}} - v_{\text{ads}} \quad (\text{S-36})$$

$$D_B \left[ \frac{\partial c_B}{\partial z} \right]_{z=0} = -v_{\text{et}} \quad (\text{S-37})$$

$$\left[ \frac{\partial \Gamma_A}{\partial t} \right] = v_{\text{ads}} \quad (\text{S-38})$$

Finally, a current response for CV,  $i_{\text{CV}}$ , is given by

$$i_{\text{CV}} = F S_{\text{el}} v_{\text{et}} \quad (\text{S-39})$$

where  $S_{\text{el}}$  is the electrode surface area.

**Dimensionless CV Model.** Diffusion equations (eq S-35) were defined by using five dimensionless parameters and solved by using a commercial finite element simulation package, COMSOL Multiphysics 5.3a. A simulated CV was fitted with an experimental CV by adjusting the dimensionless parameters as well as two scaling factors. Specifically, eq S-35 for species,  $i$  (= A or B) yielded

$$\frac{\partial C_i}{\partial \tau} = \gamma_i \left[ \frac{\partial^2 C_i}{\partial Z^2} \right] \quad (\text{S-40})$$

where

$$C_i = c_i / c_0 \quad (\text{S-41})$$

$$\tau = Fvt / RT \quad (\text{S-42})$$

$$Z = z \sqrt{\frac{Fv}{RTD_A}} \quad (\text{S-43})$$

Dimensionless parameters were also introduced for boundary conditions (eqs S-36–S-38) as

$$\left[ \frac{\partial C_A}{\partial Z} \right]_{Z=0} = V_{\text{et}}^{\text{CV}} - V_{\text{ads}}^{\text{CV}} \quad (\text{S-44})$$

$$\left[ \frac{\partial C_B}{\partial Z} \right]_{Z=0} = -\frac{V_{\text{et}}^{\text{CV}}}{\gamma_i} \quad (\text{S-45})$$

$$\left[ \frac{\partial \theta_A}{\partial \tau} \right] = \frac{V_{\text{ads}}^{\text{CV}}}{K^{\text{CV}}} \quad (\text{S-46})$$

with

$$K^{\text{CV}} = \frac{\Gamma_s}{c_0} \sqrt{\frac{Fv}{D_A RT}} \quad (\text{S-47})$$

In these equations, the ET rate was normalized to yield

$$V_{\text{et}}^{\text{CV}} = \Lambda_{\text{het}}^{\text{CV}} \left[ (\theta_{\text{ET}})^{-\alpha_{\text{ET}}} C_B - (\theta_{\text{ET}})^{1-\alpha_{\text{ET}}} C_A \right] \quad (\text{S-48})$$

with

$$\Lambda_{\text{het}}^{\text{CV}} = k_0 \sqrt{\frac{RT}{D_A Fv}} \quad (\text{S-49})$$

The adsorption rate was given in the dimensionless form as

$$V_{\text{ads}}^{\text{CV}} = \Lambda_{\text{ads}}^{\text{CV}} (\theta_{\text{ads}})^{\alpha_{\text{ads}}} C_A (1 - \theta_A) - \Lambda_{\text{dse}}^{\text{CV}} (\theta_{\text{ads}})^{\alpha_{\text{ads}}-1} \theta_A \quad (\text{S-50})$$

with

$$\Lambda_{\text{ads}}^{\text{CV}} = k_{\text{ads}}^0 \Gamma_s \sqrt{\frac{RT}{D_A Fv}} \quad (\text{S-51})$$

$$\Lambda_{\text{des}}^{\text{CV}} = k_{\text{des}}^0 \frac{\Gamma_s}{A_{\text{bulk}}} \sqrt{\frac{RT}{D_A Fv}} \quad (\text{S-52})$$

Adsorption equilibrium was achieved at  $t = 0$  to yield

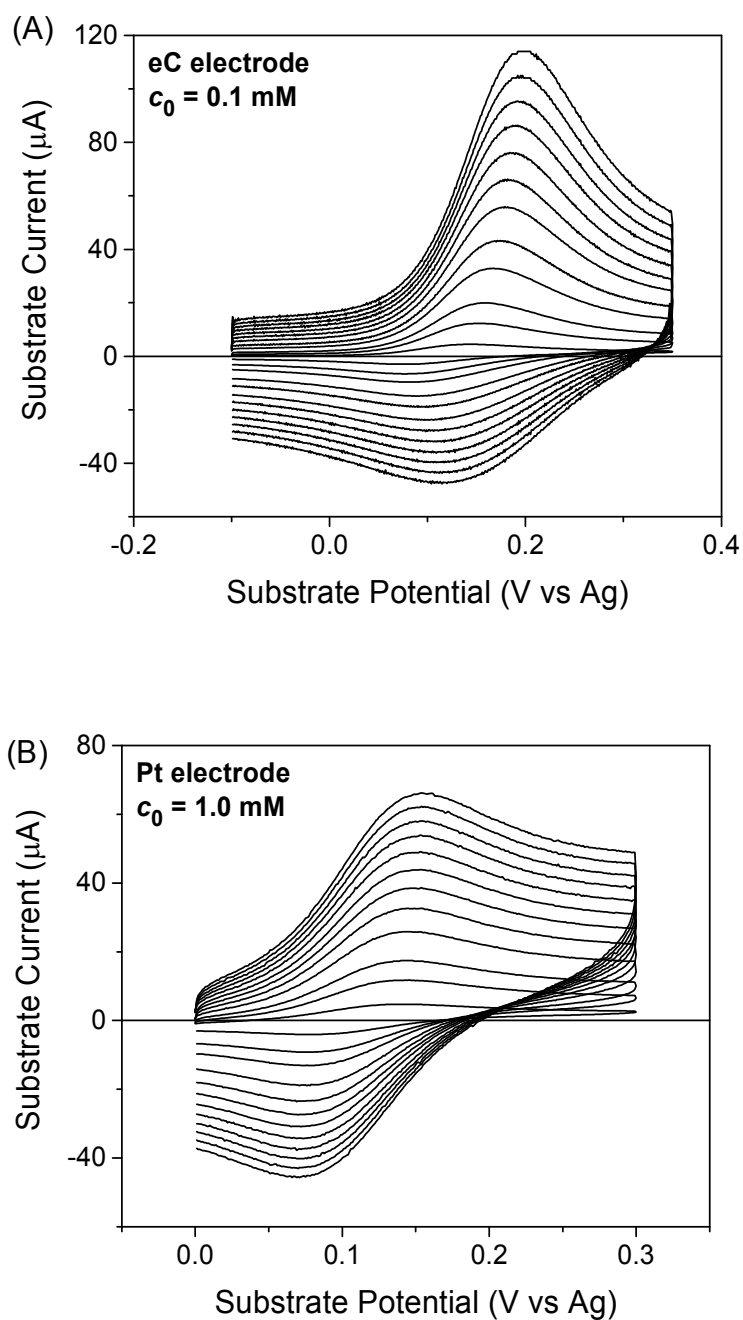
$$\frac{\Lambda_{\text{ads}}^{\text{CV}}}{\Lambda_{\text{des}}^{\text{CV}}} = \frac{\theta_A}{1 - \theta_A} \exp(-g' \theta_A) \quad (\text{S-53})$$

Overall,  $V_{\text{et}}^{\text{CV}}$  is equivalent to a normalized current response,  $I_{\text{CV}}$ , to yield

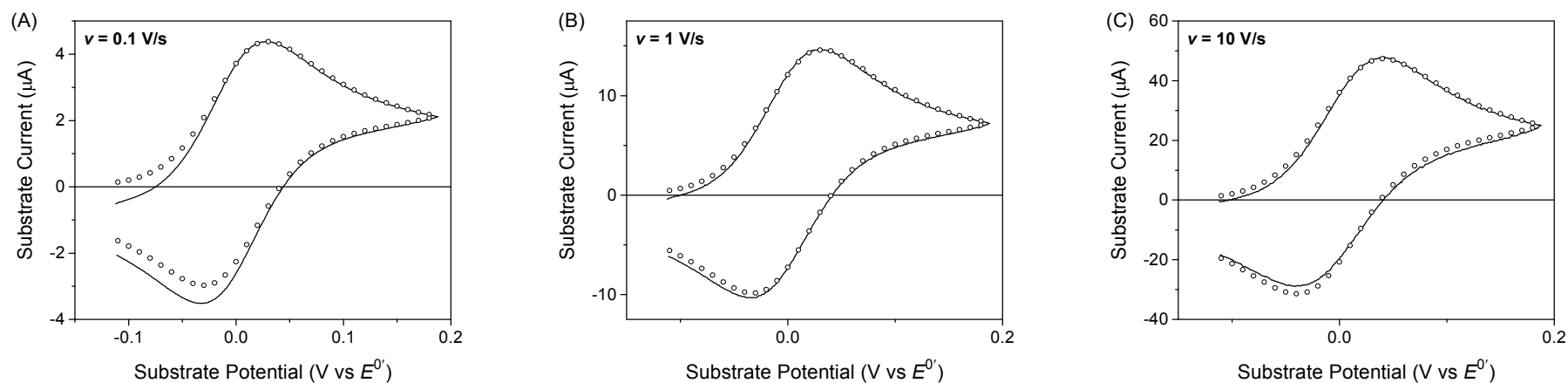
$$I_{\text{CV}} = V_{\text{et}}^{\text{CV}} = \frac{i_{\text{CV}}}{FS_{\text{el}}c_0} \sqrt{\frac{RT}{D_A Fv}} \quad (\text{S-54})$$

where  $FS_{\text{el}}c_0 \sqrt{D_A Fv / RT}$  is a scaling factor and  $V_{\text{et}}^{\text{CV}} = 0.4463$  for a reversible CV without adsorption.

**CV of  $\text{Co}(\text{phen})_3^{2+}$  at eC and Pt Electrodes.** In this work, CV of  $\text{Co}(\text{phen})_3^{2+}$  at eC (e.g., Figure S6A) and Pt (Figure S6B) electrodes was measured at potential scan rates of 0.1, 0.5, 1, 2, 3, 4, 5, 6, 7, 8, 9, and 10 V/s. Background-subtracted CVs were analyzed by the finite element method as discussed in the main text as well as in Supporting Information below. CVs with a 2 mm-diameter Pt electrode were measured only using 1.0 mM  $\text{Co}(\text{phen})_3^{2+}$  in 1 M KCl (Figure S6B) and fitted without adsorption after background subtraction (Figure S7).

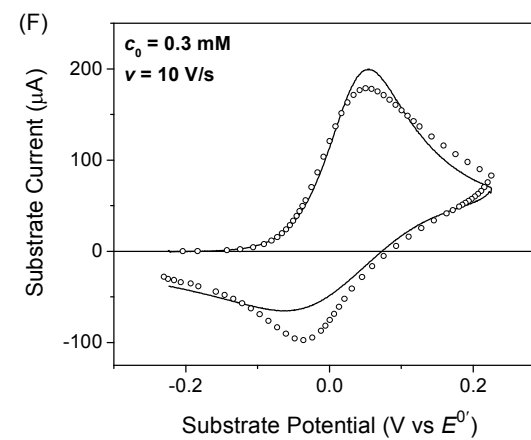
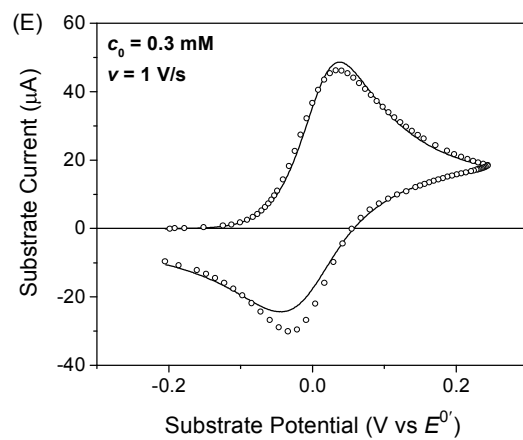
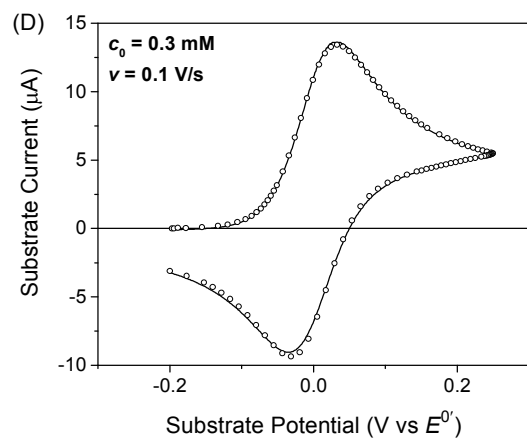
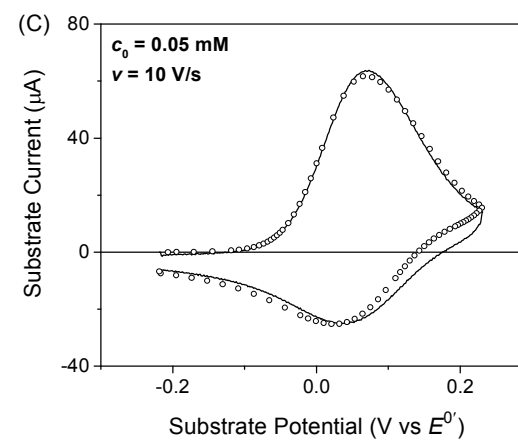
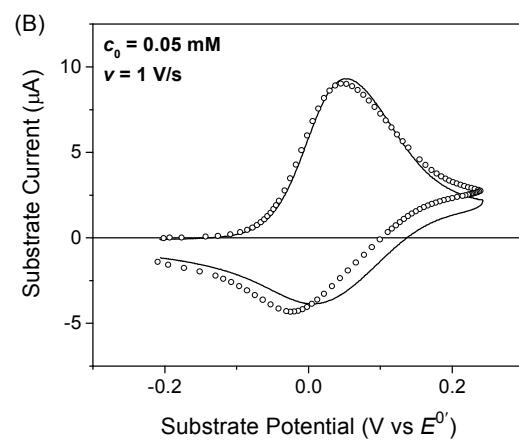
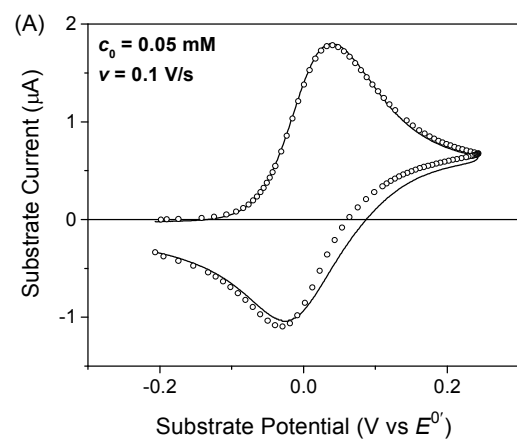


**Figure S6.** CVs of (A) 0.1 mM  $\text{Co(phen)}_3^{2+}$  at an eC electrode and (B) 1 mM  $\text{Co(phen)}_3^{2+}$  at a 2 mm-diameter Pt electrode in 1 M KCl. Potential sweep rates are 0.1, 0.5, 1, 2, 3, 4, 5, 6, 7, 8, 9, and 10 V/s.



**Figure S7.** Experimental (solid lines) and simulated (circles) CV of 1.0 mM  $\text{Co(phen)}_3^{2+}$  at a 2 mm-diameter Pt electrode in 1 M KCl. Scan rates were (A) 0.1, (B) 1, and (C) 10 V/s. No adsorption was considered in the finite element simulation, i.e.,  $k_{\text{ads}}^0 = 0$ , to yield a  $k_0$  value of 0.065 cm/s and electrode areas of  $0.031 \pm 0.002 \text{ cm}^2$ .

**CV with Different Concentrations of  $\text{Co(phen)}_3^{2+}$  and KCl.** We measured and analyzed CV of 0.05, 0.1, 0.3, and 1.0 mM  $\text{Co(phen)}_3^{2+}$  in 1 and 0.1 and 0.3 mM  $\text{Co(phen)}_3^{2+}$  in 0.1 M KCl (Figures S8 and S9, respectively) to obtain good fits with CV simulated using adsorption parameters listed in Table 1.



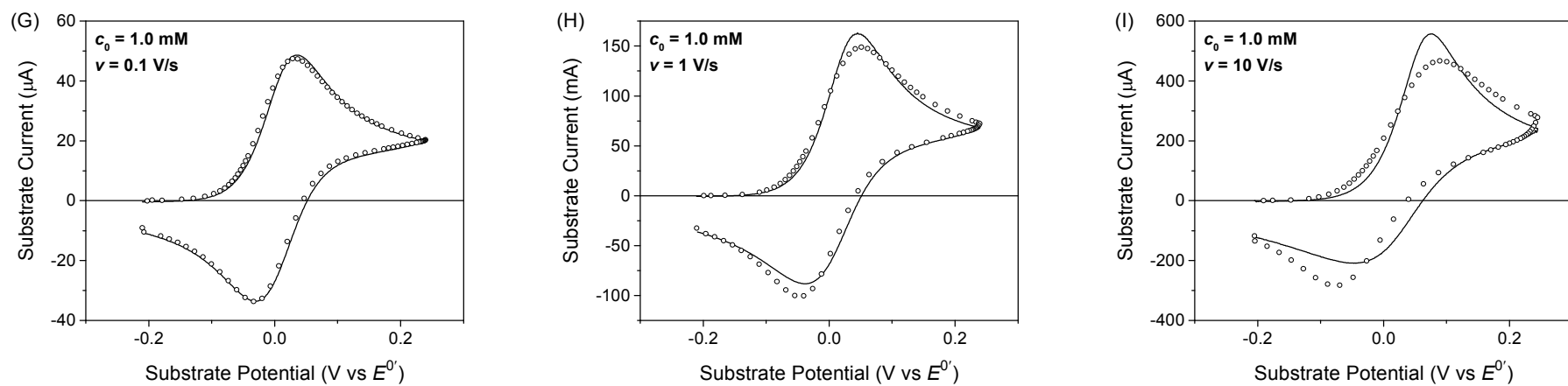


**Figure S8.** Experimental (solid lines) and simulated (circles) CV of (A–C) 0.05, (D–F) 0.3, and (G–I) 1.0 mM  $\text{Co(phen)}_3^{2+}$  at eC electrodes in 1 M KCl. Scan rates were (A, D, G) 0.1, (B, E, H) 1, and (C, F, I) 10 V/s. Fits yielded electrode areas of  $0.28 \pm 0.07$ ,  $0.31 \pm 0.02$ , and  $0.34 \pm 0.01 \text{ cm}^2$ , respectively, in addition to adsorption parameters listed in Table 1.

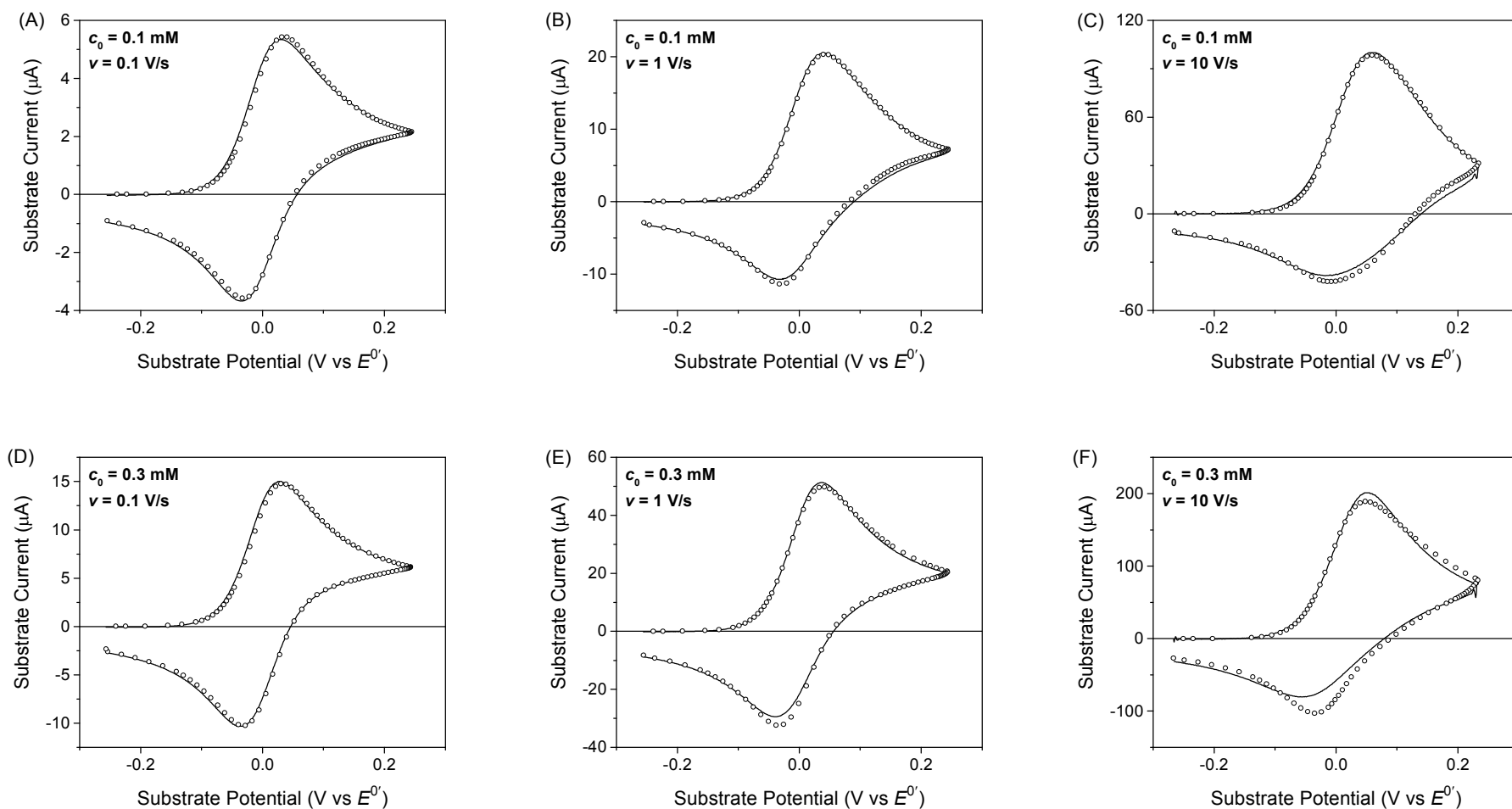


**Figure S9.** Experimental (solid lines) and simulated (circles) CV of (A–C) 0.1 and (D–F) 0.3 mM  $\text{Co}(\text{phen})_3^{2+}$  at eC electrodes in 0.1 M KCl. Scan rates were (A, D) 0.1, (B, E) 1, and (C, F) 10 V/s. Simulation employed electrode areas of  $0.36 \pm 0.03$  and  $0.34 \pm 0.01$   $\text{cm}^2$ , respectively, in addition to adsorption parameters listed in Table 1.

**Comparison of Dimensionless Parameters between SECM and CV.** Here, we compare models developed for SECM and CV based on five dimensionless parameters. Four dimensionless parameters of one model are related to those of the other model by using a scaling factor of  $a\sqrt{Fv/D_A RT}$  as given by

$$\Lambda_{\text{het}}^{\text{SECM}} = \Lambda_{\text{het}}^{\text{CV}} \left( a\sqrt{Fv/D_A RT} \right) \quad (\text{S-55})$$

$$K_{\text{SECM}} = K_{\text{CV}} / \left( a\sqrt{Fv/D_A RT} \right) \quad (\text{S-56})$$

$$\Lambda_{\text{ads}}^{\text{SECM}} = \Lambda_{\text{ads}}^{\text{CV}} \left( a\sqrt{Fv/D_A RT} \right) \quad (\text{S-57})$$

$$\Lambda_{\text{des}}^{\text{SECM}} = \Lambda_{\text{des}}^{\text{CV}} \left( a\sqrt{Fv/D_A RT} \right) \quad (\text{S-58})$$

Accordingly,

$$V_{\text{et}}^{\text{SECM}} = V_{\text{et}}^{\text{CV}} \left( a\sqrt{Fv/D_A RT} \right) \quad (\text{S-59})$$

$$V_{\text{ads}}^{\text{SECM}} = V_{\text{ads}}^{\text{CV}} \left( a\sqrt{Fv/D_A RT} \right) \quad (\text{S-60})$$

where  $V_{\text{et}}^{\text{SECM}}$  and  $V_{\text{ads}}^{\text{SECM}}$  are dimensionless ET and adsorption rates, respectively. Eqs S-59 and S-60 ensure that boundary conditions for diffusing species A and B can be scaled between SECM and CV models using  $a\sqrt{Fv/D_A RT}$ . In addition, the other dimensionless parameter,  $g' (= 2g\Gamma_s / RT)$ , is identical in both models. Nevertheless, a different scaling factor must be used for the boundary condition of adsorbed species A, where

$$\left[ \frac{\partial \theta_A}{\partial \tau} \right] = \frac{V_{\text{ads}}^{\text{SECM}}}{K_{\text{SECM}}} = \frac{V_{\text{ads}}^{\text{CV}}}{K_{\text{CV}}} \left( a\sqrt{Fv/D_A RT} \right)^2 \quad (\text{S-61})$$

Therefore, the SECM model is not exactly equivalent to the CV model with a scaling factor of

$a\sqrt{Fv/D_A RT}$ . Moreover, the mode of mass transport can be different between CV and SECM. A

SECM-based nanogap voltammogram reaches a quasi-steady state when  $a\sqrt{Fv/D_A RT} \ll 1$  with a small tip radius at a potential sweep rate where a transient current response is expected for a macroscopic substrate.

**Comparison between CV and Nanogap Voltammetry.** Excellent fits could be obtained for all CVs shown in Figure S10A–C using a single set of parameters (Table S1) for simultaneous fitting of three CVs at different scan rates (0.1, 1, 10 V/s). However, the same set of parameters caused a significant deviation between experimental and simulated nanogap voltammograms in the SG/TC mode (Figure S10D–F). Moreover, among the parameters determined by fitting CVs only, the electrode area was much smaller than an expected area of 0.28 cm<sup>2</sup>. In addition,  $\Gamma_s$  value was too large and corresponded to a radius of only 0.44 nm in eq 10 instead of an expected diameter of 0.65 nm<sup>S-1</sup> when adsorbed Co(phen)<sub>3</sub><sup>2+</sup> molecules are assumed to be spherical and closely packed. Therefore, in this work we favored a single set of parameters (Table S1) that yield best simultaneous fits for CVs and nanogap voltammograms in the SG/TC mode upon assuming that adsorption processes were fast enough to be controlled by thermodynamics only (Frumkin isotherm).

---

**Table S1. Parameters for CVs and Nanogap Voltammograms of 0.05 mM Co(phen)<sub>3</sub><sup>2+</sup> in 1 M KCl**

---

|  | Figure S10            | Figures 6A and S8A–C   |
|--|-----------------------|------------------------|
| $k_0$ (cm/s) <sup>a</sup>                | 0.38                  | 0.291                  |
| $\Gamma_s$ (mol/cm <sup>2</sup> )        | $2.5 \times 10^{-10}$ | $3.82 \times 10^{-11}$ |
| $\beta$ (L/mol)                          | $5.7 \times 10^4$     | $1.49 \times 10^5$     |
| $g'$                                     | -14.6                 | -4.6                   |
| $S_{el}$ (cm <sup>2</sup> ) <sup>b</sup> | 0.189                 | 0.28                   |

<sup>a</sup> Reversible for CV. <sup>b</sup> Used only for CV.

---

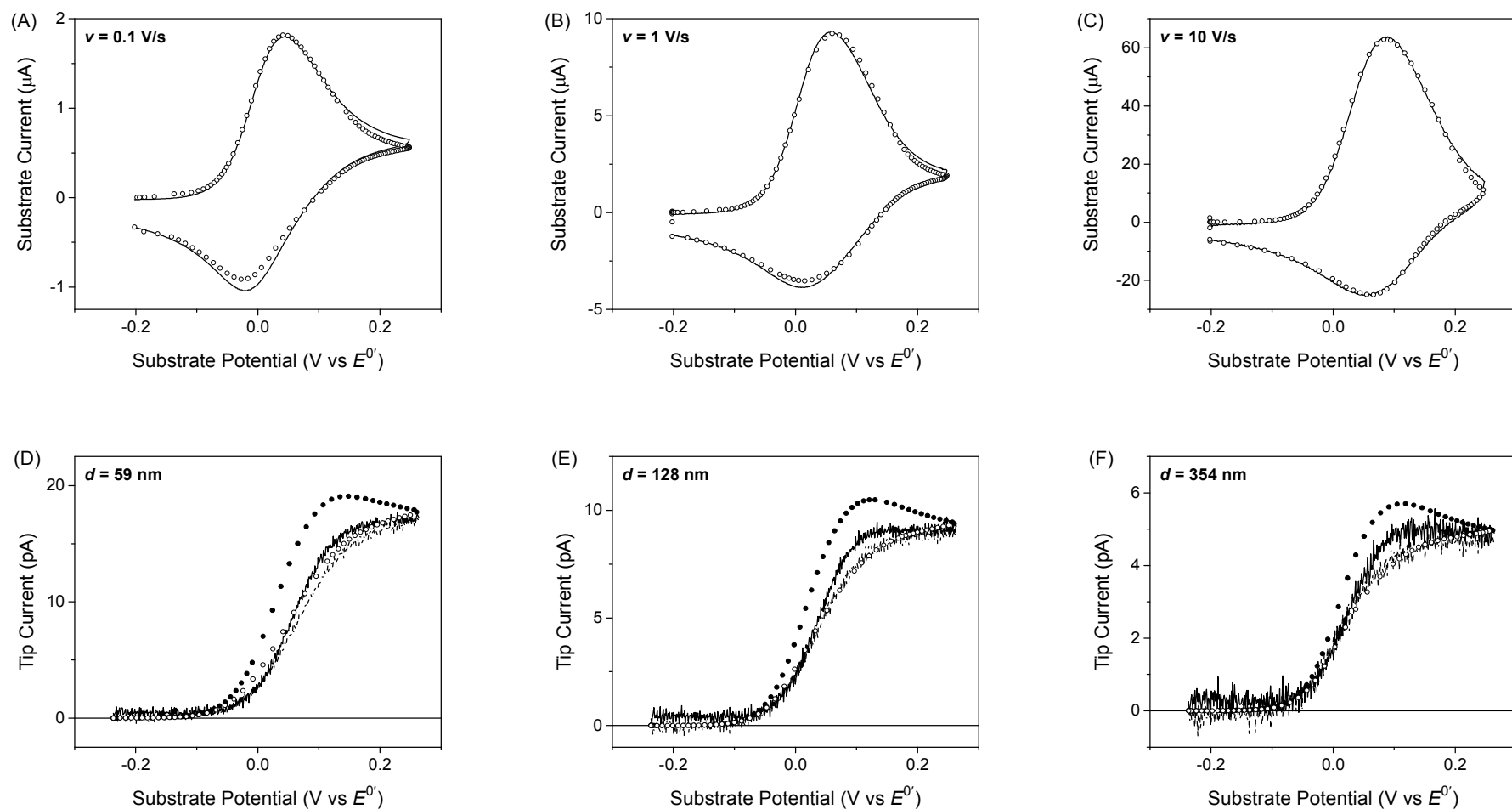


**Figure S10.** Experimental (solid) and simulated (circles) plots of (A–C) CV and (D–F) nanogap voltammograms of 0.05 mM  $\text{Co}(\text{phen})_3^{2+}$  at eC electrodes in 1 M KCl. In parts (D)–(F), solid lines and closed circles represent forward scans, whereas dashed lines and open circles correspond to reverse scans.

**Effective Sizes of Adsorbed  $\text{Co(phen)}_3^{2+}$  Molecules** We estimated the area of the eC surface occupied or blocked by each of adsorbed  $\text{Co(phen)}_3^{2+}$  molecules as follows. In this analysis, we assumed that each  $\text{Co(phen)}_3^{2+}$  molecule is represented by a sphere with an effective radius,  $r_c$ , and is closely packed on the eC surface (Figure S11) to yield

$$\theta_A \Gamma_s = 1 / 2\sqrt{3}r_c^2 N_A \quad (\text{S-62})$$

Accordingly, eq S-62 with  $\theta_A = 1$  yields eq 10 with  $r_c = r_s$  at saturation. In addition, eqs 10 and S-62 give

$$\theta_A = r_s^2 / r_c^2 \quad (\text{S-63})$$

Now, we extend the Amatore model<sup>S-2</sup> for self-inhibitory ET as follows. In the original model, a fraction of an electrode surface,  $\theta$ , is blocked by an impermeable film to yield

$$k_0 = k_0^t (1 - \theta) \quad (\text{S-64})$$

For self-inhibitor ET, the eC surface is blocked by spheres with a radius,  $r_b$ , (Figure S11) to yield

$$\theta = r_b^2 / r_c^2 \quad (\text{S-65})$$

A combination of eq S-65 with eq S-63 yields

$$\theta = (r_b / r_s)^2 \theta_A \quad (\text{S-66})$$

Eq 66 was combined with eq S-64 to yield eq 12.

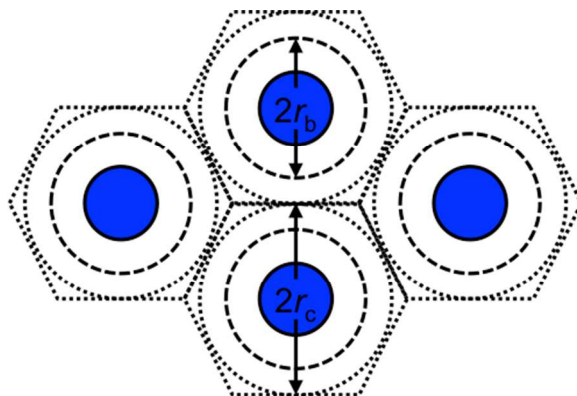


**Figure S11.** Scheme of a closely packed sphere (dotted) with an effective radius of  $r_c$  and a sphere (dashed) with a radius of  $r_b$  as a blocking layer of the eC surface. Each sphere is centered at the center of a  $\text{Co(phen)}_3^{2+}$  molecule (blue sphere with a radius of  $0.65 \text{ nm}^{\text{S-1}}$ ).

**Frumkin Correction.** The Frumkin model of double-layer effects on the ET kinetics was not able to explain linear relationships between  $k_0$  and  $\theta_A$  (Figure 7A). The Frumkin model assumes that a reactant can access the OHP at any lateral location of the electrode surface to mediate outer-sphere reaction and that the effective concentration of the reactant at the OHP is electrostatically affected by charges on the electrode surface. In this model, effective  $k_0$  was related to  $k_0^t$  by<sup>S-3</sup>

$$k_0 = k_0^t \exp\left[\frac{(\alpha - z_A)F\phi_2}{RT}\right] \quad (\text{S-67})$$

where  $z_A$  is the charge of the reactant,  $\text{Co(phen)}_3^{2+}$ , and  $\phi_2$  is the potential at the OHP. We employed the Gouy–Chapman–Stern model<sup>S-4</sup> to relate  $\phi_2$  to the charge density of  $\text{Co(phen)}_3^{2+}$  adsorbed on the eC surface as given by

$$\sigma_A \theta_A = \sqrt{8kT\varepsilon\varepsilon_0 n_0} \sinh\left(\frac{F\phi_2}{2RT}\right) \quad (\text{S-68})$$

where  $\sigma_A$  ( $= 7.4 \mu\text{C}/\text{cm}^2$ ) is the surface charge density of  $\text{Co(phen)}_3^{2+}$  at saturation,  $\varepsilon$  is the dielectric constant of solution,  $\varepsilon_0$  is the permittivity of free space,  $n_0$  is the number concentration of each ion in a

1:1 electrolyte (i.e., KCl), and the charges of the eC surface are neglected. Eq S-68 was combined with eq S-67 to yield

$$k_0 = k_0^t \left[ \frac{\sqrt{8kT\varepsilon\varepsilon_0 n^0}}{\sigma_A \theta_A + \sqrt{(\sigma_A \theta_A)^2 + 8kT\varepsilon\varepsilon_0 n^0}} \right]^{2(z_A - \alpha)} \quad (\text{S-69})$$

Eq S-69 did not fit well with a linear relationship between  $k_0$  and surface coverage when  $\alpha = 0.5$ ,  $z_A = +2$  and  $\sigma_A = 7.4 \mu\text{C}/\text{cm}^2$  were employed to yield  $k_0^t = 0.38 \text{ cm/s}$  from the best fit (Figure S12). Eq S-69 cannot produce a quick linear decay of  $k_0$  toward zero at higher surface coverage as observed experimentally.

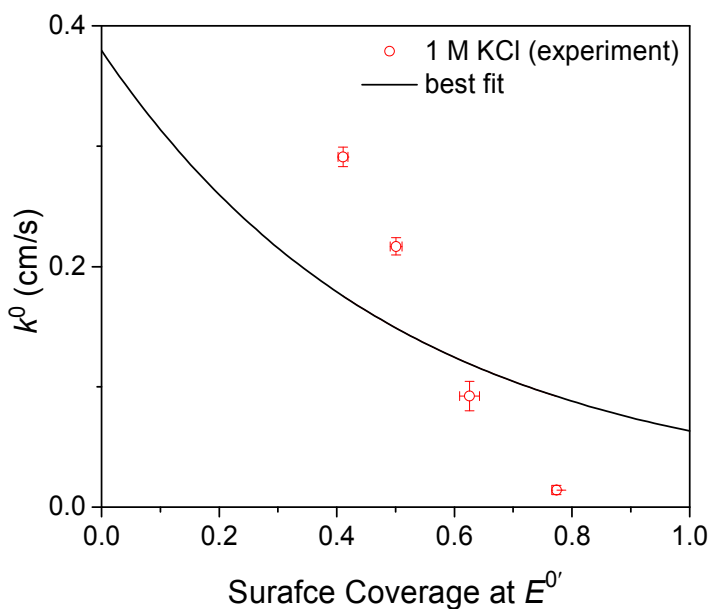


**Figure S12.** A plot of  $k_0$  versus surface coverage at  $E^{0'}$  (circles) at the eC surface in 1 M KCl as determined by SECM-based nanogap voltammetry and fitted with eq S-69 (solid).

## REFERENCES

- (S-1) Williams, M. E.; Benkstein, K. D.; Abel, C.; Dinolfo, P. H.; Hupp, J. T. *Proc. Natl. Acad. Sci. U. S. A.* **2002**, *99*, 5171.
- (S-2) Amatore, C.; Savéant, J. M.; Tessier, D. *J. Electroanal. Chem.* **1983**, *147*, 39.
- (S-3) Bard, A. J.; Faulkner, L. R. *Electrochemical Methods: Fundamentals and Applications*; 2nd ed.; John Wiley & Sons: New York, 2001, p 572.
- (S-4) Bard, A. J.; Faulkner, L. R. *Electrochemical Methods: Fundamentals and Applications*; 2nd ed.; John Wiley & Sons: New York, 2001, p 552.